


Three-body fragmentation dynamics of $\text{CH}_2\text{CCH}_2^{3+}$ investigated by 50-keV/u Ne^{8+} impactChao Ma,¹ Shenyue Xu ,^{1,*} Dongmei Zhao,^{2,3} Dalong Guo,^{2,3} Shuncheng Yan,^{2,3} Wentian Feng,^{2,3} Xiaolong Zhu,^{2,3} and Xinwen Ma^{2,3,†}¹*MOE Key Laboratory for Nonequilibrium Synthesis and Modulation of Condensed Matter, School of Science, Xi'an Jiaotong University, Xi'an 710049, China*²*Institute of Modern Physics, Chinese Academy of Sciences, Lanzhou 730000, China*³*School of Nuclear Science and Technology, University of Chinese Academy of Sciences, Beijing 100049, China*

(Received 19 December 2019; accepted 16 April 2020; published 4 May 2020)

The three-body fragmentation dynamics of triply charged allene ($\text{CH}_2\text{CCH}_2^{3+}$) induced by 50-keV/u Ne^{8+} ion impact is studied by measuring the charged fragments in coincidence using the reaction microscope. We focus on the fragmentation dynamics of two completely measured fragmentation channels, $\text{H}^+ + \text{CH}^+ + \text{C}_2\text{H}_2^+$ and $\text{H}^+ + \text{CH}_2^+ + \text{C}_2\text{H}^+$, for which breakage of one CH bond and one CC bond occurred during fragmentation. Both concerted and sequential dissociation mechanisms are observed for these two channels. For sequential process, we found that CH bond cleavage in the first step followed by CC cleavage is the major contribution for both channels. However, the process in which breakage of the CC bond is prior to CH breakage is observed for only the $\text{H}^+ + \text{CH}_2^+ + \text{C}_2\text{H}^+$ channel. The relative contributions of different fragmentation pathways are determined.

DOI: [10.1103/PhysRevA.101.052701](https://doi.org/10.1103/PhysRevA.101.052701)**I. INTRODUCTION**

The three-body fragmentation process of molecules, for which at least two chemical bonds are disrupted either simultaneously or sequentially, has attracted a tremendous amount of attention for several decades [1–35]. Most of the existing studies are performed with triatomic inorganic molecules such as CO_2 [2,6–11], CS_2 [1,2,12,13], N_2O [2,14,15], NO_2 [1], OCS [1,2,16–18], and H_2O [19] or small clusters such as N_2Ar , O_2Ar , O_2Xe [20], COAr [21], and $(\text{CO})_2$ [22]. Both concerted and sequential fragmentation mechanisms have been identified utilizing the extensively applied Newton diagrams [1,2] and Dalitz plots [36,37]. Very recently, a new representation of the experimental data named native frame was developed to disentangle the concerted and sequential processes [23,24].

Hydrocarbon molecules widely exist in the nature and play an important role in industry. The investigation of the fragmentation mechanisms of hydrocarbons is not only of fundamental interest but also important in many application fields such as plasma physics [38], the chemistry of planetary atmospheres [39], and evolution of the interstellar mediums [40]. Nevertheless, the fragmentation mechanism of hydrocarbons is far from being clear due to the fact that a hydrocarbon molecule usually consists of more than three nuclei, leading to much more complicated fragmentation mechanisms compared with the triatomic molecules. The concerted and the sequential processes were observed to play critical roles also in the fragmentation of hydrocarbon molecules, e.g., CH_4

[5,25,26], C_2H_2 [4,27–30], C_2H_4 [31,32], C_4H_6 [33], and C_6H_6 [3,34].

We choose allene (CH_2CCH_2) as the target in the present study. As shown in Fig. 1, this molecule belongs to the D_{2d} point group with three carbon atoms connected by two double bonds staying in a line while four H atoms are located in two planes which are perpendicular to each other. Several experiments were performed to investigate the ionization and fragmentation mechanisms of allene induced by ultraviolet photons [41], ions [42], electrons [43], and intense laser fields [44–47]. The isomer effect was a hot topic in these earlier studies. Direct evidence of isomer effects between allene and propyne (CHCCCH_3) was observed in the ionization and dissociation induced by C^+ ions [42] and electrons [43]. Xu *et al.* investigated the Coulomb explosion of allene induced by an ultrashort intense laser field with a pulse duration of ~ 40 fs [45–47]. Ultrafast migration of hydrogen around the skeletal structure made by three C atoms is observed not only in the two-body fragmentation of doubly charged parent ions [45] but also in the three-body fragmentation of triply charged parent ions [46,47]. Such a hydrogen migration process is also observed in the fragmentation of propyne [48,49]. In Ref. [50] the authors pointed out that hydrogen migration observed in the three-body fragmentation process should be finished before ionization of the third electron. Since three-body decomposition proceeds immediately after trications are produced, the probability of proton migration in a trication should be extremely low [50]. In addition to the experiments listed above, there are also theoretical works tracing possible dissociation pathways of allene cations with *ab initio* calculations [51,52].

In this work we investigate the three-body fragmentation of triply charged allene induced by a Ne^{8+} ion. The

*xushenyue@xjtu.edu.cn

†x.ma@impcas.ac.cn

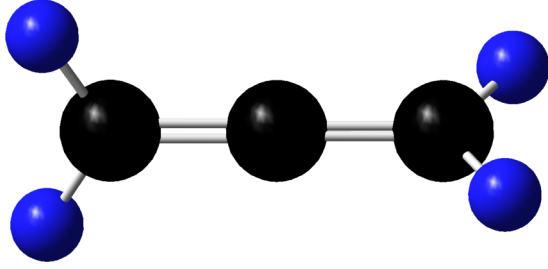


FIG. 1. Molecular structure of allene. The black and blue balls represent C and H atoms, respectively.

high-charge nature of Ne^{8+} makes it easy to remove electrons from the target. A series of experiments was performed with high-charged ions to investigate fragmentation of different molecules, such as CO_2 [6,8,10], N_2O [15], $(\text{N}_2)_2$ [53], CH_4 [26], and C_2H_2 [29]. The projectile energy in our study is chosen to be 50 keV/u, corresponding to a velocity of 1.4 a.u. With this energy the ionization occurs mainly in the outer shell [54,55]. The interaction between the projectile and the target is dominated by the projectile-nuclei-target-electron interaction, while the projectile-nuclei-target-nuclei interaction makes a negligible contribution [56]. This leads to the typical momentum transfer on the order of several atomic units [56,57], which is much smaller than the momentum of the fragments obtained from Coulomb explosion. Thus the deformation of the target by the projectile is negligible, and the structure of the precursor $\text{CH}_2\text{CCH}_2^{3+}$ produced by collision is almost the same as a neutral molecule. This is very different from ionization and dissociation induced by intense laser fields for which the interaction usually lasts for tens of femtoseconds, and mechanisms such as elongation of chemical bonds and enhanced ionization may occur before fragmentation [58,59]. Consequently, the dissociation mechanisms observed in the present work would be different from fragmentation induced by an intense laser field [46,47,50]. We will demonstrate that the concerted fragmentation process with one CH bond and one CC bond breaking simultaneously is the dominant contribution of the three-body fragmentation of $\text{CH}_2\text{CCH}_2^{3+}$, while the sequential process with two bonds breaking sequentially makes a minor contribution.

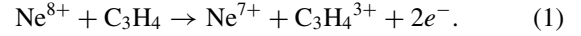
II. METHODS

A. Experimental details

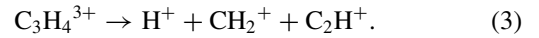
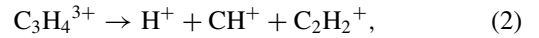
The experiment was performed using a reaction microscope (also called cold-target recoil-ion momentum spectroscopy) [57,60,61] mounted on the 320-kV platform for multidisciplinary research with highly charged ions at the Institute of Modern Physics, Chinese Academy of Sciences. Since details of the experimental method can be found in Refs. [29,57], only a short introduction is given here. Briefly, the 50-keV/u Ne^{8+} beam crosses with the allene jet produced by supersonic expansion. After collision the fragmented ions are extracted toward a position-sensitive detector by homogeneous electric field (180 V/cm) and are recorded. The scattered projectile is charge analyzed by an electrostatic deflector and detected by another position-sensitive detector

in coincidence with the ionic fragments. Residual Ne^{8+} ions without scattering are dumped into a Faraday cup.

In this study we focus on the fragmentation of the allene trication ($\text{C}_3\text{H}_4^{3+}$), which is produced through capturing one electron while ionizing the other two by the Ne^{8+} projectile, i.e., the transfer ionization process:



Different dissociation channels of $\text{CH}_2\text{CCH}_2^{3+}$ could be identified through the time-of-flight (TOF) information of the recorded fragments. Among various channels we consider the following two completely measured three-body dissociation channels:



The data presented in this paper are the quadruple coincidence events of the three ionic fragments and the scattered Ne^{7+} ion. Momentum vectors of the detected fragments are calculated according to the TOF and position information; consequently, their kinetic energies (KEs) are obtained. The overall momentum resolution in the extracting electric field, the projectile beam, and the gas jet directions are determined to be 8, 9, and 12 a.u., respectively. Momentum balance conditions are applied to eliminate the contribution of the ^{13}C isotope as well as the background noises arising from false coincidence.

B. Data presentation

We employ the Newton diagram [1,2], the Dalitz plot [36,37], and the native frame developed in Refs. [23,24] to display the correlation between the relative momentum vectors of the three fragments and to reveal details of the dissociation mechanisms.

The Newton diagram has been widely employed to reveal the momentum correlation between different fragments produced in a molecular dissociation process following the pioneering work of Eland and colleagues [1,2]. In a Newton diagram, the momentum vector of one of the three fragments is usually represented by an arrow fixed at 1.0 arbitrary unit along the x axis, while the momentum vectors of the other two fragments (C_2H_2^+ and CH^+ or C_2H^+ and CH_2^+) are normalized to this arrow and plotted in the upper and lower half planes of the diagram, respectively.

The Dalitz plot was primarily developed in particle physics by Dalitz [36,37]. In the present study the Dalitz coordinates X and Y are defined as

$$X = \frac{P_b^2 - P_a^2}{\sqrt{3} \sum P_i^2}, \quad (4)$$

$$Y = \frac{P_c^2}{\sum P_i^2} - \frac{1}{3}. \quad (5)$$

where a , b , and c represent the three detected fragments, H^+ , CH^+ , and C_2H_2^+ (or H^+ , CH_2^+ , and C_2H^+), respectively. P_i ($i \in \{a, b, c\}$) represents the momentum of each fragment in the center-of-mass frame of the allene molecule. Here the X and Y coordinates are defined as a function of P_i^2 [8,13,15,26,29] but not the KEs of the fragments as

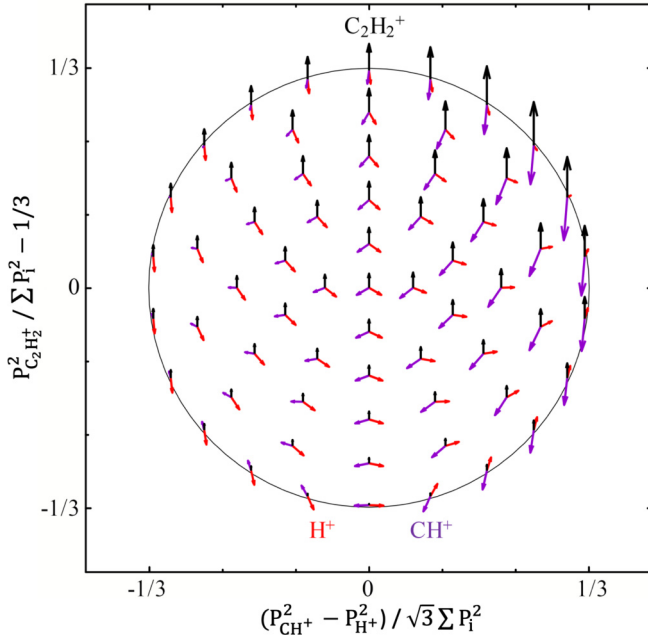


FIG. 2. Calculated momentum correlation as a function of Dalitz coordinates (X, Y) for the $H^+ + CH^+ + C_2H_2^+$ channel. The red, purple, and black arrows denote the momentum vectors of H^+ , CH^+ and $C_2H_2^+$, respectively.

in Refs. [6,9,10,14,18,36] because of the noticeably smaller mass of the proton compared with the other two fragments. Figure 2 presents the calculated momentum correlation as a function of Dalitz coordinates (X, Y) for the $H^+ + CH^+ + C_2H_2^+$ channel. As shown in Fig. 2, each point in the Dalitz plot corresponds to a specific momentum correlation pattern between the three fragments. For the $H^+ + CH_2^+ + C_2H^+$ channel, the calculated momentum correlation is similar to the correlation pattern shown in Fig. 2, with a negligible difference arising from the small mass difference between CH^+ and CH_2^+ ($C_2H_2^+$ and C_2H^+) in two distinct dissociation channels.

The advantage of the native frame developed in Refs. [23,24] is not only to reveal details of the sequential pathway of a two-step process but also to evaluate the relative contribution of this sequential pathway. In this presentation, the data are plotted as a function of KER_{INT} and the angle γ_{INT} , which are defined as the kinetic-energy release (KER) in the second step and the angle between the relative momentum vectors associated with the two steps, respectively (see Ref. [23]). INT here denotes the intermediate dication that fragments in the second step.

III. RESULTS AND DISCUSSION

A. $H^+ + CH^+ + C_2H_2^+$ channel

Figures 3(a) and 3(b) present the Newton diagram and the Dalitz plot for the $H^+ + CH^+ + C_2H_2^+$ dissociation channel, respectively. The two most intense areas appear in the upper and lower half planes of the Newton diagram shown in Fig. 3(a). These intense areas overlap with the semicircular structures marked by the blue solid semicircles. The major

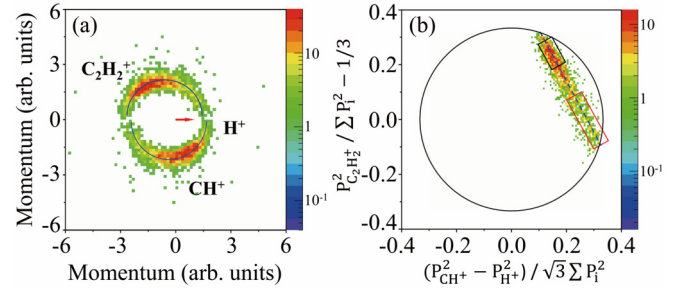
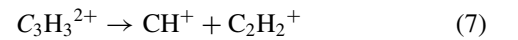
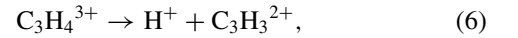


FIG. 3. (a) Newton diagram normalized to the momentum of H^+ (red arrow) for the $H^+ + CH^+ + C_2H_2^+$ channel. (b) Dalitz plot for this channel. Black and red rectangles are Dalitz filters used to deduce KE distributions shown in Fig. 4. The black rectangle covers the most intense area in the Dalitz plot with the major contribution of concerted fragmentation and a small admixture from sequential pathway I. The red rectangle covers the weakest area and contains only the contribution of pathway I. Blue solid semicircles in (a) and the dashed line in (b) are meant to guide the eye for the semicircular structure and the oblique stripe structure.

contribution of these intense regions is the concerted fragmentation process originating from the initial configuration of the CH_2CCH_2 molecule. Nevertheless, there is some admixture from other mechanisms since these intense areas overlap with the semicircular structures. The assignment of the concerted process is consistent with the Dalitz plot shown in Fig. 3(b). The most intense region in this plot is marked by the black rectangle. As can be seen in Fig. 2, the momentum correlation pattern for this region is similar to the intense regions shown in Fig. 3(a).

The semicircular structures marked by blue solid semicircles in Fig. 3(a) are typical features of the sequential fragmentation process [2] with one CH bond and one CC bond breaking sequentially. As discussed in Ref. [2], such structures indicate a sequential pathway in which the intermediate $C_3H_3^{2+}$ rotates before fragmentation. Here we denote this fragmentation process as pathway I:



in steps 1 and 2, respectively. Since the proton emitted in the first step does not lie in the line of the C skeleton, it is reasonable that the $C_3H_3^{2+}$ dication will acquire angular momentum from the repulsion of the proton and rotate. Correspondingly, the Dalitz plot in Fig. 3(b) presents an oblique stripe structure along the blue dashed line, which is also a typical feature of the sequential fragmentation process in which the intermediate dication rotates in the fragmentation plane [6,8,29]. From the momentum correlation patterns shown in Fig. 2 we could see that the mutual angle between CH^+ and $C_2H_2^+$ momenta does not change too much ($< 13^\circ$) along the blue dashed line except for the edge region. In contrast the mutual angle between H^+ and CH^+ as well as between H^+ and $C_2H_2^+$ varies dramatically. Whenever one angle increases, the other decreases. Such features of the mutual angles support the fragmentation sequence of pathway I in which the proton is produced in the first step, while CH^+ and $C_2H_2^+$ are produced

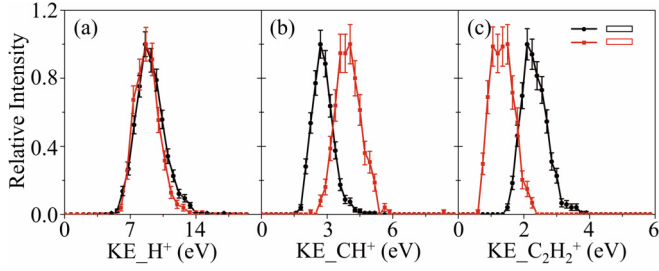


FIG. 4. KE distributions of (a) H^+ , (b) CH^+ , and (c) C_2H_2^+ with different Dalitz filters shown in Fig. 3(b). The Dalitz filter for each curve is associated by color code. These curves are normalized to unity at the maximum.

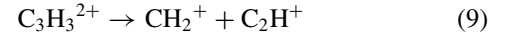
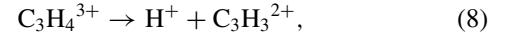
in the second step through fragmentation of the intermediate $\text{C}_3\text{H}_3^{2+}$.

To further discriminate the fragmentation mechanisms, we present in Figs. 4(a)–4(c) the KE distributions of three fragments with Dalitz filters of the black and red rectangles shown in Fig. 3(b). The KE distributions of CH^+ and C_2H_2^+ shown in Figs. 4(b) and 4(c) present an obvious dependence on the Dalitz filters. The KE of CH^+ increases as the Dalitz filter switches from the black to red rectangle, while the KE of C_2H_2^+ decreases. On the contrary, the KE distribution of H^+ shown in Fig. 4(a) does not change as the Dalitz filters and the KEs of the other two fragments vary. Such KE distributions confirm our conclusion that H^+ is produced in step 1 of the sequential process. Since H^+ attains its KE in step 1, this energy should be independent of the KEs of CH^+ and C_2H_2^+ produced in step 2 after H^+ emission.

B. $\text{H}^+ + \text{CH}_2^+ + \text{C}_2\text{H}^+$ channel

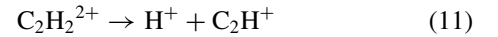
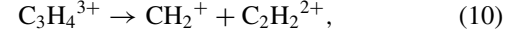
The Newton diagram [Fig. 5(a)] and the Dalitz plot [Fig. 5(b)] for the $\text{H}^+ + \text{CH}_2^+ + \text{C}_2\text{H}^+$ channel exhibit structures very similar to those of the $\text{H}^+ + \text{CH}^+ + \text{C}_2\text{H}_2^+$ channel. The major contribution of the most intense areas in these figures is attributed to the concerted process with one CH bond

and one CC bond breaking simultaneously. The semicircular structures marked by blue solid semicircles in the Newton diagram and the oblique stripe structure marked by the blue dashed line in the Dalitz plot are attributed to the sequential process which is denoted as pathway II:



in steps 1 and 2, respectively. In this sequential process the CH bond breaks prior to the CC bond, which is the same as pathway I. The assignment of the concerted process and the sequential pathway II are consistent with the KE distributions with different Dalitz filters shown in Figs. 6(a)–6(c). The KE of H^+ does not change as the Dalitz filters vary from the red to black rectangle, while KEs of the other two fragments change concomitantly, with one increasing while the other decreases.

It is worth noting that another semicircular structure with weak intensity appears in the Newton diagram marked by gray dashed semicircles in Fig. 5(a). This structure corresponds to a weak oblique stripe structure in the Dalitz plot marked by the gray rectangle in Fig. 5(b). These features indicate that another sequential fragmentation pathway alternative to pathway II occurred. In the following we will demonstrate that this pathway corresponds to the fragmentation sequence in which the cleavage of a CC bond occurs before cleavage of a CH bond, and the CH_2^+ is produced in the first step. Here we denote this fragmentation process as pathway III:



in steps 1 and 2, respectively.

Figure 5(c) presents the Newton diagram normalized to the momentum of CH_2^+ for the events inside the gray rectangle in Fig. 5(b). The semicircular structures are typical features of the sequential fragmentation process with CH_2^+ emitted in

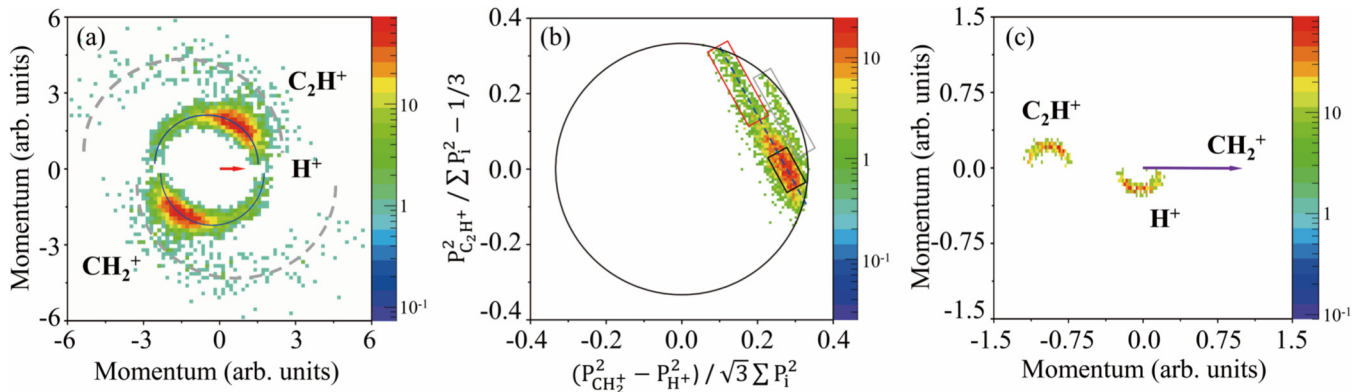


FIG. 5. (a) Newton diagram normalized to the momentum of H^+ (red arrow) for the $\text{H}^+ + \text{CH}_2^+ + \text{C}_2\text{H}^+$ channel. (b) Dalitz plot for this channel. Black, red, and gray rectangles in this plot are Dalitz filters used to deduce the Newton diagram shown in (c) and KE distributions shown in Fig. 6. The black rectangle covers the most intense area in the Dalitz plot with the major contribution of concerted fragmentation and a small admixture from sequential pathway II. The red rectangle covers the weakest area and contains only the contribution of pathway II. The gray rectangle covers another oblique stripe structure with weak intensity and contains the contribution of pathway III. Blue solid and gray dashed semicircles in (a) are meant to guide the eye for the semicircular structure, and the blue dashed line in (b) is the guidance for the oblique stripe structure. (c) Newton diagram normalized to the momentum of CH_2^+ (purple arrow) for events inside the gray rectangle in (b).

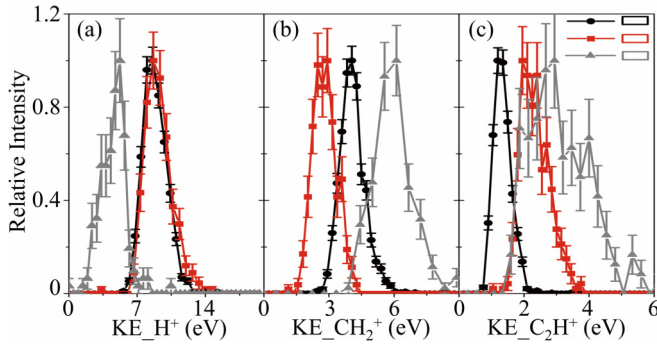
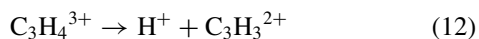


FIG. 6. KE distributions of (a) H^+ , (b) CH_2^+ , and (c) C_2H^+ with different Dalitz filters shown in Fig. 5(b). The Dalitz filter for each curve is associated by color code. These curves are normalized to unity at the maximum.

the first step while H^+ and C_2H^+ are produced in a following step. The two semicircles in Fig. 5(c) arise from the rotation of the intermediate $C_2H_2^{2+}$ in the fragmentation plane before the second step dissociation [2]. Such assignment of the fragmentation sequence of pathway III is supported by comparing the KEs of the fragments with sequential pathway II. As can be seen in Fig. 6(b), the KE of CH_2^+ from pathway III (gray line) is much higher than that from pathway II (red line), reflecting that CH_2^+ from pathway III experiences a much stronger Coulombic repulsion from the residual part of the parent ion. This is consistent with the fragmentation sequence of pathway III in which CH_2^+ is produced in step 1 and is repelled by the double-charged $C_2H_2^{2+}$. In contrast, as shown in Fig. 6(a), the KE of H^+ from pathway III is roughly a half as that from pathway II. This is because the H^+ of pathway III is emitted in step 2 and attains its KE mainly from repulsion of the single-charged C_2H^+ . The intermediate $C_2H_2^{2+}$ may obtain an amount of KE during the Coulomb repulsion with CH_2^+ in step 1. However, only a small part (1/26) of this energy is transferred to the KE of H^+ due to the small mass ratio between H^+ and C_2H^+ . Thus the KER of step 1 makes a negligible contribution to the KE of H^+ . On the contrary, C_2H^+ inherits most of the KE of the intermediate $C_2H_2^{2+}$. For the same reason, the semicircle for H^+ in Fig. 5(c) sits around the original point, while the other semicircle for C_2H^+ locates on the opposite side of the CH_2^+ momentum. The broad distribution of the KE of C_2H^+ [gray line in Fig. 6(c)] is due to the joint contribution from both step 1 and step 2.

C. Related electronic states

According to the above discussions, $C_3H_3^{2+}$ is the intermediate molecular dication of sequential pathways I and II. This is supported by the observation of the two-body fragmentation channel



in our measurement. This two-body fragmentation channel was also theoretically predicted in Ref. [51]. The existence of this channel indicates that the lifetime of the $C_3H_3^{2+}$ dication could be much longer than its rotation period (typically, ~ 10 ps) since it takes around $3 \mu s$ for $C_3H_3^{2+}$ to reach the detector.

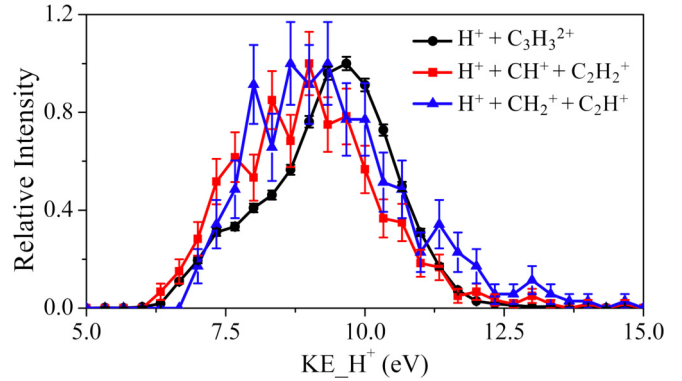


FIG. 7. KE distributions of H^+ emitted through the $H^+ + C_3H_3^{2+}$ two-body fragmentation channel and emitted during the first step of pathways I and II. These curves are normalized to unity at the maximum.

In Fig. 7 we compare the KEs of protons emitted in the first step of sequential pathway I [events inside the red rectangle in Fig. 3(b)] and pathway II [events inside the red rectangle in Fig. 5(b)] with the two-body fragmentation channel $H^+ + C_3H_3^{2+}$. Here the KE of a proton multiplied by 40/39 is the KER during the first step according to the momentum balance. As shown in Fig. 7, the KE distribution of a proton for the $H^+ + C_3H_3^{2+}$ channel exhibits shoulder and peak structures. This is consistent with the calculation in Ref. [51] that the $H^+ + C_3H_3^{2+}$ fragmentation channel may result in two different geometries of the $C_3H_3^{2+}$ product: CH_2CCH^{2+} in the 2B_2 state and $CHCHCH^{2+}$ in the ${}^2A''$ state with potential energy 1.6 eV higher than that in the 2B_2 state. Since a lower KE of a proton indicates that more energy would be deposited in the intermediate $C_3H_3^{2+}$, i.e., leading to a state of $C_3H_3^{2+}$ with a higher potential energy, the shoulder and peak structures are assigned to the ${}^2A''$ and 2B_2 states, respectively [62]. The curves for pathways I and II cover an energy range similar to that of the $H^+ + C_3H_3^{2+}$ channel, indicating that both sequential pathways may be related to the same states as the $H^+ + C_3H_3^{2+}$ two-body fragmentation channel. Following this, we suggest that CH_2CCH^{2+} in the 2B_2 state and $CHCHCH^{2+}$ in the ${}^2A''$ state as well as their vibrational excited states are the most probable states involved in sequential pathways I and II. In addition, the $C_3H_3^{2+}$ dication in the 2B_2 state with lower potential energy is expected to be more stable than the higher-lying ${}^2A''$ state. Thus one may expect that the relative contribution of the ${}^2A''$ state to the three-body fragmentation pathways I and II would be higher than the two-body dissociation channel [in Eq. (12)]. This may qualitatively explain the different shapes between the KE distribution of protons for the two-body channel [in Eq. (12)] and for pathways I [in Eqs. (6) and (7)] and II [in Eqs. (8) and (9)].

Another two-body fragmentation channel,



was predicted in Ref. [51], supporting the existence of sequential pathway III proceeding through $C_2H_2^{2+}$. However, we could not identify this channel in our measurement because such events overlap with incompletely detected coin-

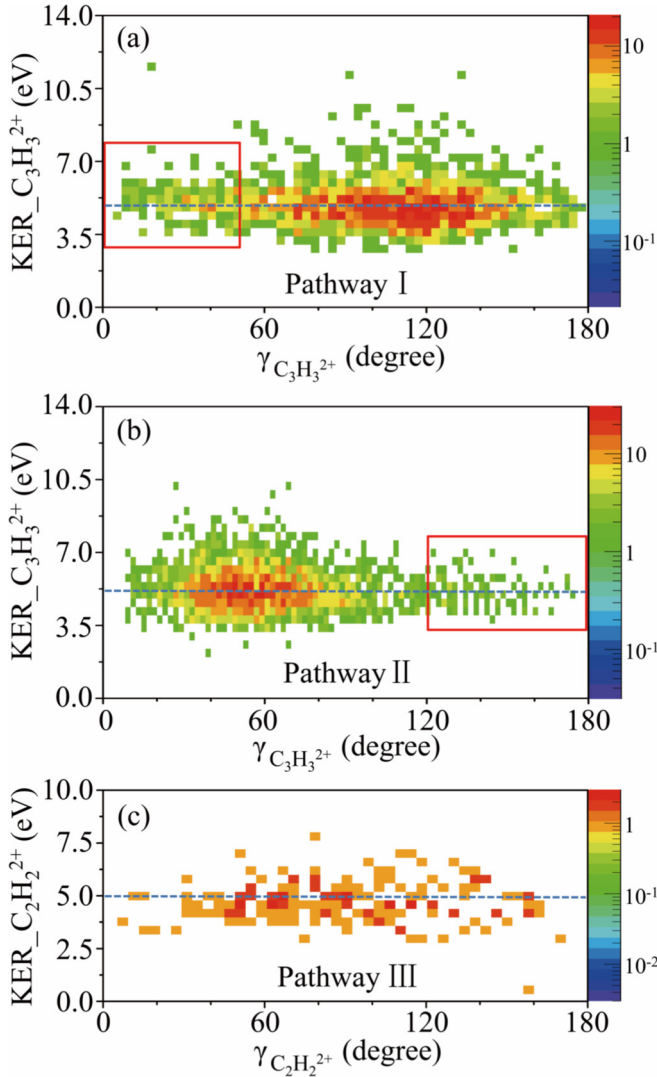


FIG. 8. The KER_{INT} vs γ_{INT} plots (a) for $\text{H}^+ + \text{CH}^+ + \text{C}_2\text{H}_2^{2+}$ events, (b) for $\text{H}^+ + \text{CH}_2^+ + \text{C}_2\text{H}^+$ events outside the gray rectangle shown in Fig. 5(b), and (c) for $\text{H}^+ + \text{CH}_2^+ + \text{C}_2\text{H}^+$ events inside the gray rectangle. Events within the red rectangles come exclusively from sequential breakup and are used to evaluate the branch ratios of sequential fragmentation channels.

cidence events $\text{CH}_2^+ + \text{CH}^+$ in the TOF correlation spectrum due to the same mass-to-charge ratio for $\text{C}_2\text{H}_2^{2+}$ and CH^+ . The signal for $\text{CH}_2^+ + \text{CH}^+$ events which could come from dissociation of the allene dication is expected to be much stronger than the $\text{CH}_2^+ + \text{C}_2\text{H}_2^{2+}$ channel from dissociation of the trication. The calculation in Ref. [51] shows that the two-body dissociation channel [in Eq. (13)] gives rise to the CCH_2^{2+} (3B_1) + CH_2^+ (2A_1) products. Thus we suggest that CCH_2^{2+} in the 3B_1 state and its vibrational excited states are the possible states of the transient $\text{C}_2\text{H}_2^{2+}$ dication involved in pathway III.

D. Relative contributions

Figures 8(a), 8(b) and 8(c) display the KER_{INT} vs γ_{INT} plots assuming that the fragmentation processes occurred through sequential pathways I, II, and III with the involved molecu-

lar intermediate $\text{C}_3\text{H}_3^{2+}$, $\text{C}_3\text{H}_3^{2+}$, and $\text{C}_2\text{H}_2^{2+}$, respectively. Figure 8(a) includes all the $\text{H}^+ + \text{CH}^+ + \text{C}_2\text{H}_2^{2+}$ events, while Figs. 8(b) and 8(c) include the $\text{H}^+ + \text{CH}_2^+ + \text{C}_2\text{H}^+$ events outside and inside the gray rectangle in Fig. 5(b), respectively. As indicated by the blue dashed lines, all three plots exhibit a band structure parallel to the horizontal axis and centered around 5 eV. The band structures in Figs. 8(a) and 8(b) overlap with the intense areas arising from concerted fragmentation processes [around 120° in Fig. 8(a) and around 60° in Fig. 8(b)]. Such band structures are consistent with sequential pathways I and II proceeding through the $\text{C}_3\text{H}_3^{2+}$ intermediate dication, while pathway III proceeds through the $\text{C}_2\text{H}_2^{2+}$ intermediate dication.

Since the lifetime of the intermediate dication $\text{C}_3\text{H}_3^{2+}$ could be much longer than its rotation period, the sequential fragmentation events through the $\text{C}_3\text{H}_3^{2+}$ intermediate dication should distribute uniformly as a function of γ . However, such a uniform distribution is disturbed in most of the γ range due to the overlap with concerted fragmentation events. Still, hints of the uniform distributions can be seen in the red rectangles in Figs. 8(a) and 8(b). The contribution of sequential fragmentation could be roughly estimated by extending the distribution in the red rectangle to the whole 0° to 180° range. The relative contribution of pathway I to the $\text{H}^+ + \text{CH}^+ + \text{C}_2\text{H}_2^{2+}$ channel is determined to be $35\% \pm 10\%$, while the relative contribution of pathway II to the $\text{H}^+ + \text{CH}_2^+ + \text{C}_2\text{H}^+$ channel is $14\% \pm 5\%$. The errors are conservatively estimated by combined consideration of the uncertainty arising from the overlap between sequential and concerted processes and the standard derivation. All the events in Fig. 8(c) are attributed to pathway III since it presents a uniform band structure. The relative contribution of pathway III to the $\text{H}^+ + \text{CH}_2^+ + \text{C}_2\text{H}^+$ channel is determined to be $6\% \pm 2\%$.

The counts and branching ratios for each fragmentation pathway of $\text{CH}_2\text{CCH}_2^{3+}$ are presented in Table I. We note that the counts of $\text{H}^+ + \text{C}_3\text{H}_3^{2+}$ shown in Table I have been corrected by a factor of 0.38 arising from different detection efficiencies of double- and triple-coincidence events [63]. The correction factor is given by the product of the open-area ratio of the microchannel plate detectors ($60\% \pm 10\%$) as a maximum detection efficiency and the transmission of two grids ($80\% \pm 10\%$ for each grid) used in the spectrometer. As clearly shown in Table I, the concerted breakup makes the major contribution to both three-body fragmentation channels. It contributes 65% to the $\text{H}^+ + \text{CH}^+ + \text{C}_2\text{H}_2^{2+}$ channel and 80% to the $\text{H}^+ + \text{CH}_2^+ + \text{C}_2\text{H}^+$ channel. The sequential fragmentation proceeding through the $\text{C}_2\text{H}_2^{2+}$ intermediate dication [pathway III, events displayed in Fig. 8(c)] makes the lowest contribution to the $\text{H}^+ + \text{CH}_2^+ + \text{C}_2\text{H}^+$ channel.

IV. CONCLUSIONS

The breakup mechanisms of two three-body fragmentation channels of allene, $\text{H}^+ + \text{CH}^+ + \text{C}_2\text{H}_2^{2+}$ and $\text{H}^+ + \text{CH}_2^+ + \text{C}_2\text{H}^+$, were investigated by $\text{Ne}^{8+} + \text{C}_3\text{H}_4 \rightarrow \text{Ne}^{7+} + \text{C}_3\text{H}_4^{3+} + 2e^-$ at 50-keV/u Ne^{8+} impact. Different decay pathways, including concerted breakup and three sequential pathways (pathways I, II, and III), were identified, and their

TABLE I. Counts and branching ratios for different fragmentation channels.

	Channel					
	$H^+ + CH^+ + C_2H_2^+$		$H^+ + CH_2^+ + C_2H^+$			$H^+ + C_3H_3^{2+}$
	Concerted	Pathway I	Concerted	Pathway II	Pathway III	
Count	1555 ± 39	853 ± 55	2656 ± 52	450 ± 37	189 ± 14	3616 ± 37
Branching ratio	$65 \pm 10\%$	$35 \pm 10\%$	$80 \pm 6\%$	$14 \pm 5\%$	$6 \pm 2\%$	

relative contributions were evaluated. The concerted breakup process in which one CH bond and one CC bond break simultaneously makes the major contribution for both three-body fragmentation channels. It contributes 65% to the $H^+ + CH^+ + C_2H_2^+$ channel and 80% to the $H^+ + CH_2^+ + C_2H^+$ channel. In pathway I the $CH_2CCH_2^{3+}$ first fragments into H^+ and the intermediate $C_3H_3^{2+}$; $C_3H_3^{2+}$ then dissociates to CH^+ and $C_2H_2^+$ in the second step. This pathway contributes 35% to the $H^+ + CH^+ + C_2H_2^+$ dissociation channel. Pathway II corresponds to the process in which the intermediate $C_3H_3^{2+}$ dissociates to CH_2^+ and C_2H^+ in the second step. This pathway comprises 14% of the $H^+ + CH_2^+ + C_2H^+$ events. The CH bond breaks prior to the CC breakage for both pathways I and II. In addition, we observed pathway III, in which the CC bond breakage occurs prior to the CH breakage. In this pathway $CH_2CCH_2^{3+}$ fragments into CH_2^+ and the

$C_2H_2^{2+}$ intermediate dication, and $C_2H_2^{2+}$ then dissociates to H^+ and C_2H^+ in the second step. It contributes 6% to the $H^+ + CH_2^+ + C_2H^+$ channel.

ACKNOWLEDGMENTS

The authors acknowledge the 320-kV platform staff at the Institute of Modern Physics, Chinese Academy of Sciences for their technical support. The work was supported by the National Key Research and Development Program of China under Grant No. 2017YFA0402300, the National Natural Science Foundation of China under Grants No. U1432122 and No. 11674332, the China Post-doctoral Science Foundation under Grant No. 2017M613100, and the Fundamental Research Funds for the Central Universities of China.

- [1] J. Eland, *Mol. Phys.* **61**, 725 (1987).
- [2] S. Hsieh and J. H. D. Eland, *J. Phys. B* **30**, 4515 (1997).
- [3] P. J. Richardson, J. H. D. Eland, and P. Lablanquie, *Org. Mass. Spectrom.* **21**, 289 (1986).
- [4] R. Thissen, J. Delwiche, J. M. Robbe, D. Dufloy, J. P. Flament, and J. H. D. Eland, *J. Chem. Phys.* **99**, 6590 (1993).
- [5] I. Ben-Itzhak, K. D. Carnes, S. G. Ginther, D. T. Johnson, P. J. Norris, and O. L. Weaver, *Phys. Rev. A* **47**, 3748 (1993).
- [6] N. Neumann, D. Hant, L. P. H. Schmidt, J. Titze, T. Jahnke, A. Czasch, M. S. Schöffler, K. Kreidi, O. Jagutzki, H. Schmidt-Böcking, and R. Dörner, *Phys. Rev. Lett.* **104**, 103201 (2010).
- [7] C. Wu, C. Wu, D. Song, H. Su, Y. Yang, Z. Wu, X. Liu, H. Liu, M. Li, Y. Deng, Y. Liu, L.-Y. Peng, H. Jiang, and Q. Gong, *Phys. Rev. Lett.* **110**, 103601 (2013).
- [8] A. Khan, L. C. Tribedi, and D. Misra, *Phys. Rev. A* **92**, 030701(R) (2015).
- [9] E. Wang, X. Shan, Z. Shen, M. Gong, Y. Tang, Y. Pan, K.-C. Lau, and X. Chen, *Phys. Rev. A* **91**, 052711 (2015).
- [10] S. Yan, X. L. Zhu, P. Zhang, X. Ma, W. T. Feng, Y. Gao, S. Xu, Q. S. Zhao, S. F. Zhang, D. L. Guo, D. M. Zhao, R. T. Zhang, Z. K. Huang, H. B. Wang, and X. J. Zhang, *Phys. Rev. A* **94**, 032708 (2016).
- [11] H. J. Yang, E. Wang, W. X. Dong, M. Gong, Z. Shen, Y. Tang, X. Shan, and X. Chen, *Phys. Rev. A* **97**, 052703 (2018).
- [12] A. Hishikawa, H. Hasegawa, and K. Yamanouchi, *Chem. Phys. Lett.* **361**, 245 (2002).
- [13] R. Guillemin, P. Declève, M. Stener, C. Bomme, T. Marin, L. Journel, T. Marchenko, R. Kushawaha, K. Jänkälä, N. Trcera, K. Bowen, D. Lindle, M. Piancastelli, and M. Simon, *Nat. Commun.* **6**, 6166 (2015).
- [14] P. Bhatt, R. Singh, N. Yadav, and R. Shanker, *Phys. Rev. A* **86**, 052708 (2012).
- [15] A. Khan, L. C. Tribedi, and D. Misra, *Phys. Rev. A* **96**, 012703 (2017).
- [16] M. R. Jana, B. Ray, P. N. Ghosh, and C. P. Safvan, *J. Phys. B* **43**, 215207 (2010).
- [17] K. Saha, S. Banerjee, and B. Bapat, *Chem. Phys. Lett.* **607**, 85 (2014).
- [18] Z. Shen, E. Wang, M. Gong, X. Shan, and X. Chen, *J. Chem. Phys.* **145**, 234303 (2016).
- [19] R. Singh, P. Bhatt, N. Yadav, and R. Shanker, *J. Phys. B* **46**, 085203 (2013).
- [20] J. Wu, M. Kunitski, L. P. H. Schmidt, T. Jahnke, and R. Dörner, *J. Chem. Phys.* **137**, 104308 (2012).
- [21] X. Gong, M. Kunitski, L. P. H. Schmidt, T. Jahnke, A. Czasch, R. Dörner, and J. Wu, *Phys. Rev. A* **88**, 013422 (2013).
- [22] X. Ding, M. Haertelt, S. Schlauderer, M. S. Schuurman, A. Yu. Naumov, D. M. Villeneuve, A. R. W. McKellar, P. B. Corkum, and A. Staudte, *Phys. Rev. Lett.* **118**, 153001 (2017).
- [23] J. Rajput, T. Severt, B. Berry, B. Jochim, P. Feizollah, B. Kaderiya, M. Zohrabi, U. Ablikim, F. Ziaee, K. Raju P., D. Rolles, A. Rudenko, K. D. Carnes, B. D. Esry, and I. Ben-Itzhak, *Phys. Rev. Lett.* **120**, 103001 (2018).
- [24] H. Kumar, P. Bhatt, C. P. Safvan, and J. Rajput, *J. Chem. Phys.* **148**, 064302 (2018).
- [25] R. Flammini, M. Satta, E. Fainelli, G. Alberti, F. Maracci, and L. Avaldi, *New J. Phys.* **11**, 083006 (2009).
- [26] Y. Zhang, T. Jiang, L. Wei, D. Luo, X. Wang, W. Yu, R. Hutton, Y. Zou, and B. Wei, *Phys. Rev. A* **97**, 022703 (2018).
- [27] A. Hishikawa, A. Matsuda, M. Fushitani, and E. J. Takahashi, *Phys. Rev. Lett.* **99**, 258302 (2007).

- [28] S. De, J. Rajput, A. Roy, P. N. Ghosh, and C. P. Safvan, *Phys. Rev. A* **77**, 022708 (2008).
- [29] S. Xu, X. L. Zhu, W. T. Feng, D. L. Guo, Q. Zhao, S. Yan, P. Zhang, D. M. Zhao, Y. Gao, S. F. Zhang, J. Yang, and X. Ma, *Phys. Rev. A* **97**, 062701 (2018).
- [30] T. Jiang, B. Wang, Y. Zhang, L. Wei, S. Chen, W. Yu, Y. Zou, L. Chen, and B. Wei, *Phys. Rev. A* **100**, 022705 (2019).
- [31] S. H. Lee, Y. T. Lee, and X. Yang, *J. Chem. Phys.* **120**, 10983 (2004).
- [32] X. Xie, E. Lötstedt, S. Roither, M. Schöffler, D. Kartashov, K. Midorikawa, A. Baltuska, K. Yamanouchi, and M. Kitzler, *Sci. Rep.* **5**, 12877 (2015).
- [33] L. Zhang, S. Roither, X. Xie, D. Kartashov, M. Schöffler, H. Xu, A. Iwasaki, S. Gräfe, T. Okino, K. Yamanouchi, A. Baltuska, and M. Kitzler, *J. Phys. B* **45**, 085603 (2012).
- [34] A. Matsuda, M. Fushitani, R. D. Thomas, V. Zhaunerchyk, and A. Hishikawa, *J. Phys. Chem. A* **113**, 2254 (2009).
- [35] E. Wang, X. Shan, Z. Shen, M. Gong, Y. Tang, and X. Chen, *J. Chem. Phys.* **151**, 134308 (2019).
- [36] R. H. Dalitz, *Philos. Mag. (1798-1977)* **44**, 1068 (1953).
- [37] R. H. Dalitz, *Phys. Rev.* **94**, 1046 (1954).
- [38] R. K. Janev, *Atomic and Molecular Processes in Fusion Edge Plasmas* (Plenum, New York, 1995).
- [39] P. V. Sada, G. L. Bjoraker, D. E. Jennings, G. H. McCabe, and P. N. Romani, *Icarus* **136**, 192 (1998).
- [40] A. G. G. M. Tielens, *Rev. Mod. Phys.* **85**, 1021 (2013).
- [41] A. C. Parr, A. J. Jason, and R. Stockbauer, *Int. J. Mass Spectrom. Ion Phys.* **26**, 23 (1978).
- [42] T. Kusakabe, S. Satoh, H. Tawara, and M. Kimura, *Phys. Rev. Lett.* **87**, 243201 (2001).
- [43] S. W. J. Scully, V. Senthil, J. A. Wyer, M. B. Shah, E. C. Montenegro, M. Kimura, and H. Tawara, *Phys. Rev. A* **72**, 030701(R) (2005).
- [44] C. Cornaggia, *Phys. Rev. A* **52**, R4328(R) (1995).
- [45] H. Xu, T. Okino, and K. Yamanouchi, *Chem. Phys. Lett.* **469**, 255 (2009).
- [46] H. Xu, T. Okino, and K. Yamanouchi, *J. Chem. Phys.* **131**, 151102 (2009).
- [47] H. Xu, T. Okino, and K. Yamanouchi, *Appl. Phys. A* **104**, 941 (2011).
- [48] T. Okino, A. Watanabe, H. Xu, and K. Yamanouchi, *Phys. Chem. Chem. Phys.* **14**, 4230 (2012).
- [49] T. Okino, A. Watanabe, H. Xu, and K. Yamanouchi, *Phys. Chem. Chem. Phys.* **14**, 10640 (2012).
- [50] T. Okino and K. Yamanouchi, in *Ultrafast Phenomena in Molecular Sciences: Femtosecond Physics and Chemistry*, edited by R. de Nalda and L. Bañares (Springer, Cham, 2014), pp. 49–60.
- [51] A. Mebel and A. Bandrauk, *J. Chem. Phys.* **129**, 224311 (2008).
- [52] B. T. Psciuk, P. Tao, and H. B. Schlegel, *J. Phys. Chem. A* **114**, 7653 (2010).
- [53] A. Méry, A. N. Agnihotri, J. Douady, X. Fléchar, B. Gervais, S. Guillous, W. Iskandar, E. Jacquet, J. Matsumoto, J. Rangama, F. Ropars, C. P. Safvan, H. Shiromaru, D. Zanuttini, and A. Cassimi, *Phys. Rev. Lett.* **118**, 233402 (2017).
- [54] M. Rødbro, E. Horsdal Pedersen, C. L. Cocke, and J. R. Macdonald, *Phys. Rev. A* **19**, 1936 (1979).
- [55] J. Matsumoto, A. Leredde, X. Flechar, K. Hayakawa, H. Shiromaru, J. Rangama, C. L. Zhou, S. Guillous, D. Hennecart, T. Muranaka, A. Mery, B. Gervais, and A. Cassimi, *Phys. Rev. Lett.* **105**, 263202 (2010).
- [56] M. S. Schöffler, J. Titze, L. P. H. Schmidt, T. Jahnke, N. Neumann, O. Jagutzki, H. Schmidt-Böcking, R. Dörner, and I. Mančev, *Phys. Rev. A* **79**, 064701 (2009).
- [57] X. Ma, R. T. Zhang, S. F. Zhang, X. L. Zhu, W. T. Feng, D. L. Guo, B. Li, H. P. Liu, C. Y. Li, J. G. Wang, S. C. Yan, P. J. Zhang, and Q. Wang, *Phys. Rev. A* **83**, 052707 (2011).
- [58] T. Seideman, M. Y. Ivanov, and P. B. Corkum, *Phys. Rev. Lett.* **75**, 2819 (1995).
- [59] S. Roither, X. Xie, D. Kartashov, L. Zhang, M. Schöffler, H. Xu, A. Iwasaki, T. Okino, K. Yamanouchi, A. Baltuska, and M. Kitzler, *Phys. Rev. Lett.* **106**, 163001 (2011).
- [60] J. Ullrich, R. Moshhammer, A. Dorn, R. Dörner, L. P. H. Schmidt, and H. Schmidt-Böcking, *Rep. Prog. Phys.* **66**, 1463 (2003).
- [61] R. Dörner, V. Mergel, O. Jagutzki, L. Spielberger, J. Ullrich, R. Moshhammer, and H. Schmidt-Böcking, *Phys. Rep.* **330**, 95 (2000).
- [62] Y. Li, S. Xu, D. Guo, S. Jia, X. Jiang, X. Zhu, and X. Ma, *J. Chem. Phys.* **150**, 144311 (2019).
- [63] B. Gaire, S. Y. Lee, D. J. Haxton, P. M. Pelz, I. Bocharova, F. P. Sturm, N. Gehrken, M. Honig, M. Pitzer, D. Metz, H.-K. Kim, M. Schöffler, R. Dörner, H. Gassert, S. Zeller, J. Voigtsberger, W. Cao, M. Zohrabi, J. Williams, A. Gatton, D. Reedy, C. Nook, T. Müller, A. L. Landers, C. L. Cocke, I. Ben-Itzhak, T. Jahnke, A. Belkacem, and T. Weber, *Phys. Rev. A* **89**, 013403 (2014).